Comparison of hydrogen determination with X-ray and neutron crystallography in a human aldose reductase–inhibitor complex

ARTICLE *in* EUROPEAN BIOPHYSICS JOURNAL · OCTOBER 2006

Impact Factor: 2.22 · DOI: 10.1007/s00249-006-0064-8 · Source: PubMed

6 AUTHORS, INCLUDING:

Flora Meilleur
North Carolina State University
53 PUBLICATIONS **563** CITATIONS
SEE PROFILE

Dean A A Myles
Oak Ridge National Laboratory
108 PUBLICATIONS **1,645** CITATIONS
SEE PROFILE

Eur Biophys J (2006) 35: 577–583
DOI 10.1007/s00249-006-0064-8

ARTICLE

M. P. Blakeley · A. Mitschler · I. Hazemann
F. Meilleur · D. A. A. Myles · A. Podjarny

Comparison of hydrogen determination with X-ray and neutron crystallography in a human aldose reductase–inhibitor complex

Received: 6 February 2006 / Accepted: 22 March 2006 / Published online: 19 April 2006

Abstract Protonation states determination by neutron (2.2 Å at room temperature) and X-ray (0.66 Å at 100 K) crystallographic studies were compared for a medium size enzyme, human aldose reductase (MW = 36 kDa), complexed with its $NADP^+$ coenzyme and a selected inhibitor of therapeutic interest. The neutron resolution could be achieved only with the ab initio fully deuterated protein and the subsequent crystallization in D_2O of the complex. We used the largest good-quality crystal ($1.00 \times 0.67 \times 0.23$ mm, i.e. volume of 0.15 mm^3) that we were able to grow so far. Both studies enable the determination of protonation states, with a clear advantage for neutrons in the case of less-ordered atoms ($B > 5$ $Å^2$). Hydrogen atoms are best determined by a complementary analysis of the Fourier maps obtained from both methods.

Introduction

Hydrogen atoms are involved in many biochemical reactions during protein function; for example, enzymatic redox reactions usually involve a proton transfer. Therefore, the understanding of structure-function relationships and the 3D design of drugs of therapeutic interest requires the knowledge of protonation states for the protein, water molecules and ligands, especially those in active sites.

However, protonation states cannot be reliably predicted at a given pH for a specific residue, as the pKa value of a particular residue strongly depends on its environment of other residues (Harris 2002). Moreover, this value cannot be simply extrapolated from the value found in solution by Raman and infrared spectroscopy (Ames and Mathies 1990; Dioumaev 2001). Direct observation of hydrogen atoms by X-ray crystallography is one option. However, the hydrogen positions and occupancies cannot be easily obtained, due to the weakness of the diffraction signal for the hydrogen atom itself (no core electron and a single bond electron). The signal cannot be easily enhanced by increasing the X-ray dose, as doses have to be kept low (even at 100 K) to minimize radiation-induced damage. In short, very high quality crystals diffracting to high resolution (better than 1 Å) on one of the best in-class synchrotron beamlines, e.g. (Rosenbaum et al. 2006), are in general needed to observe hydrogen atoms (Dauter et al. 1997; Esposito 2002; Petrova and Podjarny 2004; Schmidt and Lamzin 2002). The protonation states have been determined at high resolution only in a very small number of proteins, e.g. for concanavalin A (0.94 Å resolution; Deacon et al. 1997), in which 52% of the main chain hydrogen atoms were seen and TEM-1 beta-lactamase (0.85 Å resolution; Minasov 2002), where 70% of the hydrogen atoms were seen.

Another option is neutron crystallography. Since neutrons interact with the atomic nuclei independently of the number of electrons, D atoms diffract neutrons with a signal of the same order of magnitude as non-hydrogen atoms. Therefore, neutron diffraction is a very appropriate tool for directly visualizing protonation states. The complementarity of neutron macromolecular crystallography and ultra-high-resolution X-ray protein crystallography has already been discussed (Habash et al. 2000). In order to perform a neutron crystallography study, very large (> 1 mm^3)

M. P. Blakeley
EMBL, 6 Rue Jules Horowitz, BP 181 Cedex 9,
38042 Grenoble, France

A. Mitschler · I. Hazemann · A. Podjarny (✉)
IGBMC, CNRS/INSERM/ULP, 1 Rue Laurent Fries,
67404 Strasbourg-Illkirch, France
E-mail: podjarny@titus.u-strasbg.fr

F. Meilleur
ILL, 6 Rue Jules Horowitz, BP 156, 38042 Grenoble, France

D. A. A. Myles
Oak Ridge National Laboratory, PO Box 2008, MS6100,
Oak Ridge, TN 37831, USA

single crystals are required to compensate for the weak flux of neutron beams. For example, the protonation states of key residues in endothiapepsin were identified using neutron data to 2.1 Å at room temperature from two crystals of 3 mm^3 (Coates et al. 2001). Such unusually large crystal volumes remain a stringent bottleneck in Structural Biology. This can be overcome in two complementary ways; the development of new incoming spallation neutron sources and the growth in D_2O of ab initio fully deuterated crystals (Shu et al. 2000; Meilleur et al. 2004; Hazemann et al. 2005; Budayova-Spano et al. 2006).

As observed in endothiapepsin, the partial H/D exchange does not alter the 3D structure (root-mean-square deviation of 0.2 Å; Coates et al. 2001). This is also true for the full substitution of all hydrogen atoms by deuterium (root-mean-square deviation of 0.1 Å for all Cα atoms; M. P. Blakeley and F. Ruiz et al. 2006, paper in preparation). On the other hand, full deuteration has a drastic positive effect on neutron scattering, since for a protein structure (including the surrounding ordered solvent) more than half of the atoms are hydrogen atoms. Therefore, full deuteration increases the coherent neutron scattering and at the same time decreases the incoherent background, thus providing an order of magnitude improvement in data rates (smaller crystals, shorter exposure times) for a similar signal-to-noise ratio in experimental frames. Moreover, no radiation-induced damage is detectable in neutron diffraction, so data can be collected at room temperature on crystals of good mosaicity, free from possible harmful effects of cryo-protectants. Thus, contrary to X-ray diffraction at synchrotrons, neutron diffraction provides a unique non-destructive tool even at room temperature.

Here, we describe the use of neutron diffraction of fully deuterated crystals of the complex human aldose reductase (h-AR)—coenzyme $NADP^+$–IDD594 to obtain structural results at room temperature with an unusually small crystal (see Neutron data collection and processing). These results are compared with those obtained from X-ray data at ultra-high resolution (0.66 Å) and 100 K (Howard et al. 2004), in particular for the determination of the hydrogen/deuterium atomic positions and occupancies.

Experimental: the case of aldose reductase

X-ray crystallography studies

Human aldose reductase (EC 1.1.1.21) is a 316 amino-acid enzyme (MW = 36 kDa). It belongs to the aldo-ketoreductase super-family, and reduces a wide range of substrates, such as aldehydes, aldoses, and corticosteroids. The enzyme reduces glucose into sorbitol, in the first step of the "polyol pathway" for glucose metabolism. Normally, this pathway is a minor one, but in hyperglycaemic conditions, it takes up to one-third of the overall glucose turnover, and therefore it has been linked to diabetic complications; h-AR remains, therefore, an ongoing target for structure-based drug design.

The crystal structure of the ternary complex of h-AR, its coenzyme $NADP^+$ and the inhibitor IDD594 was solved and refined against diffraction data at 0.66 Å at 100 K (Howard et al. 2004), with a final R factor of 9.4% (R-free:10.3%) for all reflections. The electron density maps showed clear density for all non-hydrogen atoms. The atom types could be unambiguously assigned by the electron density values around them in many regions of the protein, as well as the cofactor and inhibitor. The hydrogen atoms were sought in $F_o - F_c$ difference maps with hydrogens omitted (OMIT-H map). They were counted as observed when the residual electron density had a value larger than 1σ at the expected hydrogen position. The percentage of observed hydrogens was found to be linearly correlated with the temperature factor of the atoms to which the hydrogen is covalently bound (correlation coefficient of 0.97 for the B range 3–11 $Å^2$; Fig. 5), e.g. 77% of hydrogen atoms are seen in the well-ordered active site ($\langle B \rangle$ = 3.4 $Å^2$) vs. 54% for all the protein ($\langle B \rangle$ = 6.9 $Å^2$).

Neutron crystallography studies

Neutron data collection and processing

The production of the fully deuterium-labelled protein sample of h-AR, its co-crystallization in D_2O with the coenzyme NADPH and inhibitor IDD594 and subsequent neutron data collection and processing have been already described (Hazemann et al. 2005). Following the protocol developed at the ILL/EMBL deuteration laboratory (Meilleur et al. 2004, 2005), h-AR was overexpressed as a His-tagged protein using a pET 28b plasmid (*Novagen*), in *Escherichia Coli* strain BL21 (DE3) (*Novagen*). Cells were adapted to fully deuterated media, and grown to high cell density in a 2 L bioreactor (*Infors*) at 30°C using a deuterated minimal medium The deuterated enzyme was purified in hydrogenated (H_2O) buffers (yield ~ 40 mg/L). The protein was concentrated to 30 mg/mL in D_2O and mixed with co-factor NADPH (dissolved in D_2O) and inhibitor IDD594 (dissolved in DMSO; protein:coenzyme:inhibitor ratio = 1:2:2). Crystallization conditions in D_2O were closely similar to those used for the hydrogenated complex (Howard et al. 2004). Micro-seeding at high dilution using pre-equilibrated hanging drops (25 μL) yielded crystals of average dimensions of 1 × 0.6 × 0.3 mm^3.

One of these crystal of dimensions 1.0 × 0.67 × 0.23 mm (i.e. volume = 0.15 mm^3, unusually small for neutron diffraction) was used for neutron Laue data collection at room temperature on the LADI instrument (Cipriani et al. 1996; Myles et al. 1998). Using a restricted neutron wavelength range ($\delta\lambda/\lambda$ = 25%) centered at 3.3 Å and extending from 2.9 to 3.7 Å, data were recorded in a series of contiguous Laue images with a step separation of φ = 7° around the

horizontal rotation axis of the camera. Spots were observed to 2.0 Å resolution, a clear improvement from the 4.5 Å resolution observed previously from a partially deuterated D_2O-soaked h-AR crystal (which had a similar volume of 0.15 mm^3).

Neutron Laue data were indexed and integrated using the Daresbury Laboratory LAUEGEN software suite (Helliwell 1989; Campbell 1995), modified for the cylindrical geometry of the LADI detector (Campbell et al. 1998). The LSCALE program (Arzt 1999) was used to derive the wavelength-normalization curve (Fig. 1) using the intensities of symmetry-equivalent reflections measured at different wavelengths. SCALA (Collaborative Computational Project, number 4, 1994) was used to combine and merge the observed 46,319 reflections to produce a final data set of 11,885 unique reflections to 2.2 Å resolution with an overall merging R factor of 22.8% (12.4% at low to 27.1% at high resolution) and $\langle I/\sigma(I)\rangle$ = 5.1 (2.9 in the outer shell) with completeness 73.5% (57.6% in the outer shell) and multiplicity 3.9 (2.7 in the outer shell; Fig. 2).

Neutron refinement

The refined room temperature X-ray structure of per-deuterated h-AR [hAR(D)] in complex with $NADP^+$ and the inhibitor IDD594 to 1.75 Å resolution (M. P. Blakeley and F. Ruiz et al. 2006, paper in preparation) was used as the starting model for the neutron refinement using CNS (Brünger 1998). Neutron scattering lengths (*International Tables for Crystallography*, 1995, Vol. *C*, pp. 384–391) were used in these calculations and the parameters used in the dictionary files of CNS were altered for neutron scattering. Firstly, all water molecules were removed from the X-ray structure and all D atoms (except those for the side chains of aspartate, glutamate, histidine, tyrosine, threonine, and serine residues) were generated for the protein and placed at stereochemically defined positions according to the algorithm in the generate script of CNS.

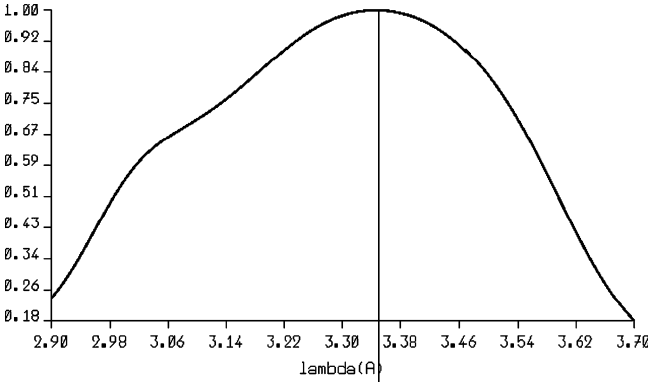

Fig. 1 The wavelength normalization curve for the neutron data set to 2.2 Å resolution

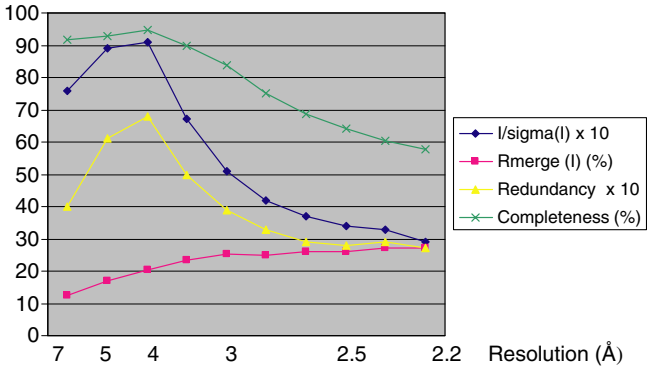

Fig. 2 Summary of the 2.2 Å neutron Laue diffraction data statistics. For a summary of the 0.66 Å X-ray data see Howard et al. 2004

The exchangeable H atoms of $NADP^+$ (seven exchangeable H atoms) and IDD594 (one exchangeable H atom) were also generated and given the scattering length for deuterium. All B factors were reset to 20 $Å^2$. A 20-cycle rigid body refinement, using all the neutron data to 2.2 Å was first performed. At this stage the R factor was 31.9% and the R-free 33.4%. Next, 10 cycles of positional refinement for all the D atoms of the protein, $NADP^+$ and IDD594 improved the R factor to 30.7% and the R-free to 31.5%. B factor refinement for all the atoms further improved the R factor to 28.5% with R-free of 30.8%. At this point the positions of the D atoms of the aspartate, glutamate, histidine, tyrosine, threonine, and serine residues were identified using the $F_o - F_c$ difference maps. Thus, the protonation states for each of amino-acid residues within h-AR were determined. Figures 3 and 4 show examples for well-ordered side chains His 83 and Thr 113 ($B \leq 5$ $Å^2$) where protonation states are clearly seen and agree with the observations in the X-ray difference maps.

D_2O molecules were included very carefully only after the construction of the entire protein structure. $F_o - F_c$ maps were used to identify possible water sites using the water-picking procedure in CNS. Water oxygen atoms were assigned if they satisfied certain distance restraints and had positive $F_o - F_c$ map σ values of greater than 3.5. The water positions identified were included in the model and positional and B factor refinement of them performed. $2F_o - F_c$ maps were checked in order to verify the fit to the nuclear density. Those water sites that displayed only weak positive nuclear density were removed and only those water sites that were clearly visible at 1.5 r.m.s in the $2F_o - F_c$ maps were ultimately included. One-hundred and fifty five water molecules were finally assigned as full D_2O molecules i.e. with strong positive nuclear density and the characteristic 'boomerang' shape density, while a further 41 water molecule positions that displayed only spherical density were included but allocated as single O atoms. The final R factor for the neutron structure was 26% and R-free 32%.

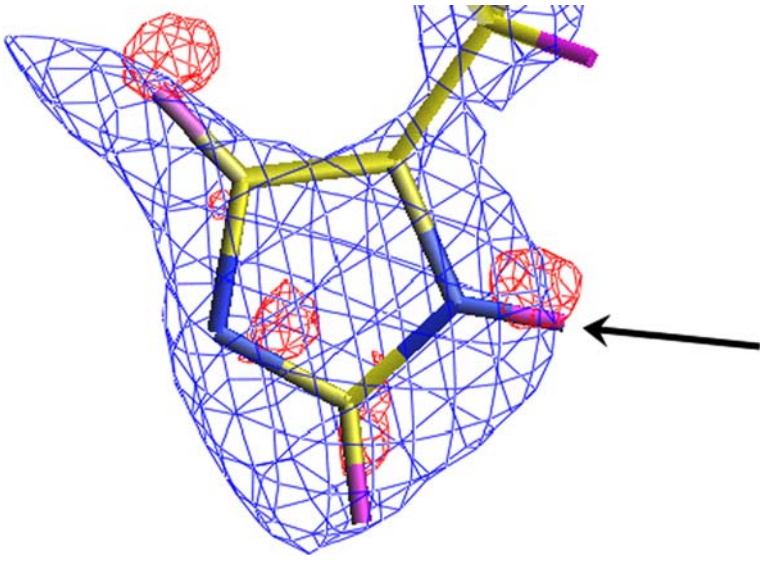

Fig. 3 The h-AR(D)-NADPH-IDD594 neutron model superposed with the $2F_o - F_c$ (D-omit, 1.5σ contour) nuclear density in *blue* at 2.2 Å and $F_o - F_c$ (H-omit, 2.3σ contour) electron density in *red* at 0.66 Å for histidine 83. Note that the H/D atom (indicated by an *arrow*) bound to the ND1 nitrogen atom ($B \sim 5$ Å^2) is clearly indicated in both maps. The slight difference between the positions of the peaks in the X-ray map and the D positions in the neutron structure corresponds to a true difference in the fractional coordinates, as the two structures are collected at different temperatures. The X-ray model is omitted for clarity reasons

Results: hydrogen isotope visibility

By analysis of the neutron Fourier $F_o - F_c$ difference maps, calculated with the D atoms omitted, we assessed the visibility of the deuterium atoms of the protein as a function of the B factor of the atom to which they are bound. In order to classify whether the D atoms were visible or not, we used the definition that a D atom was visible if it had a Fourier peak at a level of 1σ or higher in the $F_o - F_c$ (D-omit) map. This was performed for all D atoms of the protein. As can be seen from Fig. 5, even at reasonably high B factors of ~ 12 Å^2 around 50% of the D atoms remain visible at a level of 1σ or better in the neutron Fourier difference maps.

Comparing these results to those from the X-ray data set at 0.66 Å (Howard et al. 2004) we can see that for a given B factor, the neutron data at medium resolution is

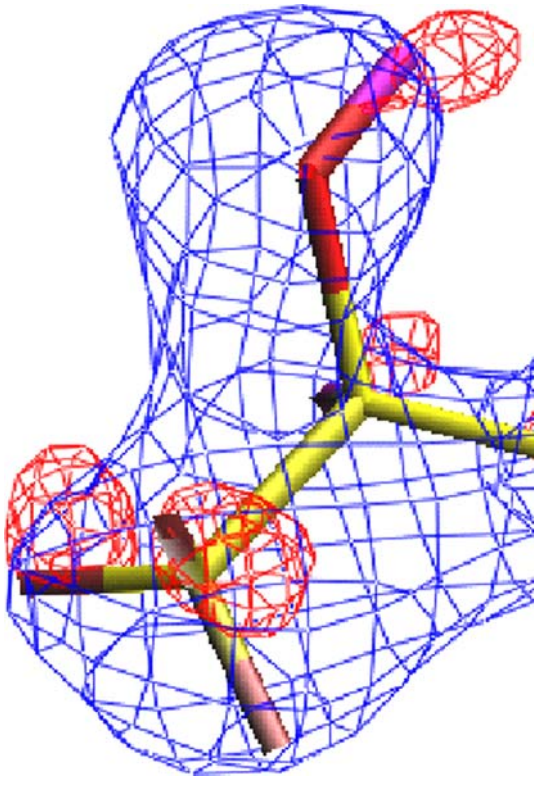

Fig. 4 The $2F_o - F_c$ (D-omit, 1.5σ contour) nuclear density in *blue* at 2.2 Å and $F_o - F_c$ (H-omit, 3σ contour) electron density in *red* at 0.66 Å for the side chain of threonine 113 in the h-AR(D)-NADPH-IDD594 complex. Note that the orientation of the O–D group is clearly observed

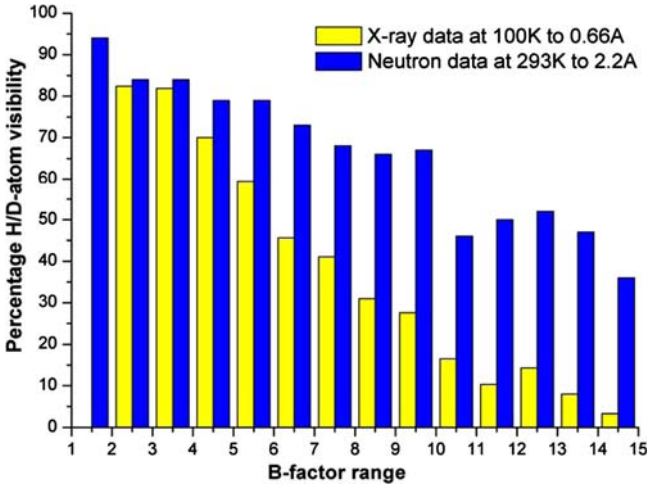

Fig. 5 *Yellow* plot of the percentage H atom visibility (using a sigma level of 1.0 in the $F_o - F_c$ H-omit maps) for the X-ray data at 0.66 Å as a function of the X-ray model B factor of the atom to which the H atom is bound. *Blue* plot of the percentage D atom visibility (using a sigma level of 1.0 in the $F_o - F_c$ D-omit maps) for the neutron Laue data at 2.2 Å as a function of the neutron model B factor of the atom to which the D atom is bound. Note that for a given atom, B neutrons $\sim 1.5B$ X-ray. Therefore, a given atom will have significantly different B factors in the two refinements, and will contribute to different histogram bars

more efficient for visualizing D atoms than the ultra-high-resolution X-ray data. As the *B* factor of the atom to which the D atom is bound increases, the fall-off in visibility is much more pronounced for the X-ray data than for the neutron data.

To refine the comparison of the observation of H atoms in the X-ray maps with the observation of D atoms in neutron maps, we need to take into account additional factors, as follows:

1. The *B* factors of the neutron structure measured at room temperature are higher than *B* factors of the X-ray structure measured at 100 K (B neutrons $\sim 1.5B$ X-ray), which implies that the histograms shown in Fig. 5 compare observations from different atoms.
2. The σ values calculated from the omit-D map are artificially high, since the deletion of all D atoms (half of the scattering power) introduces additional noise.
3. The 1σ level cutoff used in Fig. 5 reflects adequately the observation of the H/D atoms, but not the strength of the observed signal. Therefore, we recalculated the percentage of D (neutrons) and H (X-rays) atoms observed as a function of the same *B* factor (from the X-ray structure determination), recalculated the σ values of the omit-D map by omitting randomly only 14% of the D atoms (to have an effect similar to omitting H atoms in the X-ray difference maps), and calculated the histograms for 1.5σ and 3σ cutoffs. The resulting histograms are shown in Figs. 6 and 7.

In summary, Fig. 5 shows the ideal impact of neutron vs. X-ray signals in deuterium/hydrogen visibility, and Figs. 6 and 7 show the real impact in the case described here. On one hand, the stronger signal from neutron maps is dampened by the higher *B* factors at room temperature, which means that the X-ray observations are better for the very low *B* factors. On the other hand, the X-ray signal decays very rapidly with increasing *B* factor, and this effect is accentuated when we look at the strongest signals (Fig. 7). Overall, the stronger signal effect overtakes the increase of the *B* factors. At the 1.5σ level, the neutron structure determines 61% of all D atoms, while the X-ray structure determines 52 % of all H-positions.

An example of this difference is shown in Fig. 8, where the D atom linked to the CE1 carbon of His 240 ($B \sim 7$ Å^2) is clearly seen in the neutron map and weakly seen in the X-ray map, where it is at the level of noise. Note that in both cases the observation of protonation states is strongly handicapped for residues with multiple conformations (99 residues out of 316 identified clearly at 100 K by X-ray diffraction).

Conclusions and perspectives

Full deuteration has drastically improved the capability of neutron crystallography. Using this technique in the h-AR case (MW = 36 kDa), even a small crystal size

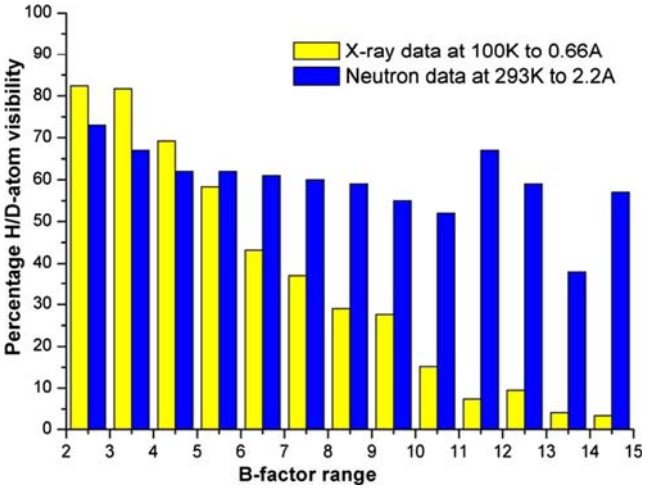

Fig. 6 *Yellow* plot of the percentage H atoms observed above a cutoff level of 1.5σ in the $F_o - F_c$ H-omit maps, for the X-ray data at 0.66 Å as a function of the X-ray model *B* factor of the atom to which the H atom is bound. *Blue* plot of the percentage D atoms observed above a cutoff level of 1.5σ (recalculated) in the $F_o - F_c$ D-omit maps, for the neutron Laue data at 2.2 Å as a function of the X-ray model *B* factor of the atom to which the D atom is bound. Note that in this case the same *B* factor is used for both cases, so that this histogram shows the difference in visibility for a given atom

(0.15 mm^3) provided good-quality neutron data to 2.2 Å resolution. The analysis of the resulting $F_o - F_c$ (D-omit) maps showed clearly the deuterium atoms, with a level of observation equal to or better than that of

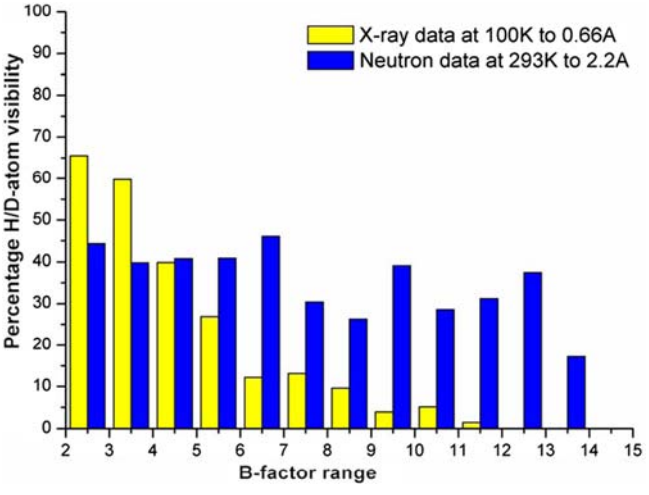

Fig. 7 *Yellow* plot of the percentage H atom observed above a cutoff level of 3.0σ in the $F_o - F_c$ H-omit maps for the X-ray data at 0.66 Å as a function of the X-ray model *B* factor of the atom to which the H atom is bound. *Blue* plot of the percentage D atom observed above a cutoff level of 3.0σ (recalculated) in the $F_o - F_c$ D-omit maps for the neutron Laue data at 2.2 Å as a function of the X-ray model *B* factor of the atom to which the D atom is bound. Note that in this case the same *B* factor is used for both cases, so that this histogram shows the difference in visibility for a given atom

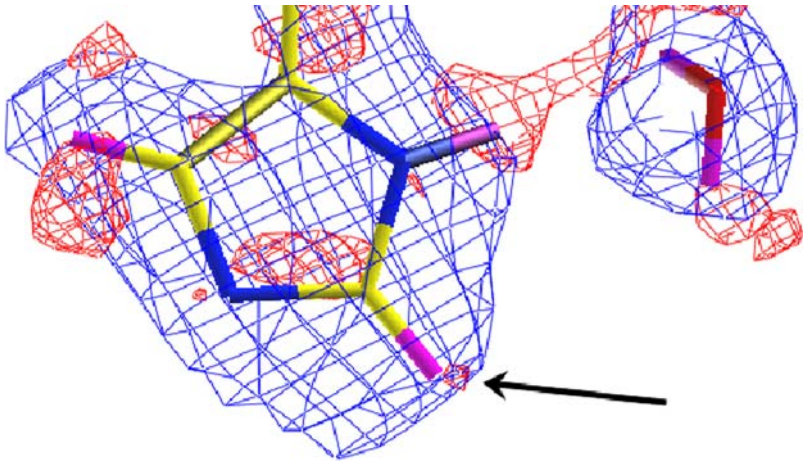

Fig. 8 The h-AR(D)-NADPH-IDD594 neutron model superposed with the $2F_o - F_c$ (D-omit, 1.2σ contour) nuclear density in *blue* at 2.2 Å and $F_o - F_c$ (H-omit, 1.5σ contour) electron density in *red* at 0.66 Å for histidine 240 and one D_2O molecule. Note that the H/D atom (indicated by an *arrow*) bound to the CE1 carbon ($B \sim 8$ Å^2) appears clearly in the neutron map and weakly in the X-ray map

the ultra-high-resolution X-ray maps, especially for the less-ordered (high *B* factor) atoms. Furthermore, the combination of both techniques is very useful for the validation of protonation states in cases where the signal is poor. The consequences for the catalytic mechanism and for structure-based drug design will be published later (M. P. Blakeley and F. Ruiz et al. 2006, paper in preparation).

In order to further improve the observation of protonation states, we are working on increasing the crystal size to achieve a higher resolution. Another important factor is to lower the temperature of the neutron data collection (Blakeley et al. 2004). With both improvements, the observation of protonation states with neutron diffraction should go significantly beyond the level obtained by ultra-high-resolution X-ray diffraction at low temperatures.

Acknowledgements We thank the staff of the EMBL and ILL, Grenoble, France and of the SBC, APS, Argonne, USA, for their help in data collection, and of the IGBMC for their support. This work was supported by the Centre National de la Recherché Scientifique (CNRS), by the CNRS-DFG collaboration (CERC3), by the Institut National de la Santé et de la Recherché Médicale and the Hôpital Universitaire de Strasbourg (H.U.S).

References

Ames J, Mathies R (1990) The role of back-reactions and proton uptake during the N–O transition in bacteriorhodopsin's photocycle: a kinetic resonance Raman study. Biochemistry 29:7181–7190

Arzt S, Campbell JW, Harding MM, Hao Q, Helliwell JR (1999) LSCALE—the new normalization, scaling and absorption correction program in the Daresbury Laue software suite. J Appl Cryst 32:554–562

Blakeley MP, Kalb (Gilboa) AJ, Helliwell JR, Myles DAA (2004) The 15-K neutron structure of saccharide-free concanavalin A. PNAS 101(47):16405–16410

Brünger AT, Adams PD, Clore GM, DeLano WL, Gros P, Grosse-Kunstleve RW, Jiang J-S, Kuszewski J, Nilges M, Pannu NS, Read RJ, Rice LM, Simonson T, Warren GL (1998) Crystallography & NMR system: a new software suite for macromolecular structure determination. Acta Cryst D54:905–921

Budayova-Spano M, Fisher S, Dauvergne M, Agbandje-McKenna M, Silverman D, Myles D, McKenna R (2006) Production and X-ray crystallographic analysis of fully deuterated human carbonic anhydrase II. Acta Crystallogr F Biol Crystallogr 62:6–9

Campbell JW (1995) LAUEGEN, an X-windows-based program for the processing of Laue X-ray diffraction data. J Appl Cryst 28:228–236

Campbell J, Hao Q, Harding M, Nguti ND, Wilkinson C (1998) LAUEGEN version 6.0 and INTLDM. J Appl Cryst 31:496–502

Cipriani F, Castagna J, Wilkinson C, Oleinek P, Lehmann M (1996) Cold neutron protein crystallography using a large position-sensitive detector based on image-plate technology. J Neutron Res 4:79–85

Coates L, Erskine P, Wood S, Myles D, Cooper J (2001) A neutron Laue diffraction study of endothiapepsin: implications for the aspartic proteinase mechanism. Biochemistry 40:13149–13157

Dauter Z, Lamzin V, Wilson K (1997) The benefits of atomic resolution. Curr Opin Struct Biol 7:681–688

Deacon A, Gleichmann T, Kalb (Gilboa) AJ, Price H, Raftery J, Bradbrook G, Yariv J, Helliwell JR (1997) The structure of concanavalin A and its bound solvent determined with small-molecule accuracy at 0.94 Å resolution. J Chem Soc Faraday Trans 93(24):4305–4312

Dioumaev A (2001) Infrared methods for monitoring the protonation state of carboxylic amino acids in the photocycle of bacteriorhodopsin. Biochemistry (Mosc) 66:1269–1276

Esposito L, Vitagliano L, Mazzarella L (2002) Recent advances in atomic resolution protein crystallography. Protein Pept Lett 9:95–106

Habash J, Raftery J, Nuttall R, Price H, Wilkinson C, Kalb AJ, Helliwell JR (2000) Direct determination of the positions of the deuterium atoms of the bound water in -concanavalin A by neutron Laue crystallography. Acta Crystallogr D Biol Crystallogr 56:541–50

Harris TK, Turner GJ (2002) Structural basis of perturbed pKa values of catalytic groups in enzyme active sites. IUBMB Life 53:85–98

Hazemann I, Dauvergne M, Blakeley M, Meilleur F, Haertlein M, Van Dorsselaer A, Mitschler A, Myles D, Podjarny A (2005) High-resolution neutron protein crystallography with radically small crystal volumes: application of perdeuteration to human aldose reductase. Acta Crystallogr D Biol Crystallogr 61:1413–1417

Helliwell JR, Habash J, Cruickshank DW, Harding MM, Greenhough TJ, Campbell JW, Clifton IJ, Elser M, Machin PA, Papiz MZ, Zurch S (1989) The recording and analysis of synchrotron X-radiation Laue diffraction photographs. J Appl Cryst 22:483–497

Howard EI, Sanishvili R, Cachau RE, Mitschler A, Chevrier B, Barth P, Lamour V, Van Zandt M, Sibley E, Bon C, Moras D, Schneider TR, Joachimiak A, Podjarny A (2004) Ultrahigh resolution drug design I: details of interactions in human aldose reductase-inhibitor complex at 0.66 Å. Proteins 55:792–804

Meilleur F, Contzen J, Myles D, Jung C (2004) Structural stability and dynamics of hydrogenated and perdeuterated cytochrome P450cam (CYP101). Biochemistry 43:8744–8753

Meilleur F, Dauvergne MT, Schlichting I, Myles DAA (2005) Production and X-ray crystallographic analysis of fully deuterated cytochrome P450cam. Acta Crystallogr D Biol Crystallogr 61:539–544

Minasov F, Wang X, Shoichet BK (2002) An ultrahigh resolution structure of TEM-1 beta-lactamase suggests a role for Glu166 as the general base in acylation. J Am Chem Soc 124:5333–5340

Myles D, Bon C, Langan P, Cipriani F, Castagna JC, Lehmann MS, Wilkinson C (1998) Neutron Laue diffraction in macromolecular crystallography. Physica B 241–243:1122–1130

Petrova T, Podjarny A (2004) Protein crystallography at subatomic resolution. Rep Prog Phys 67:1565–1605

Rosenbaum G, Alkire R, Evans G, Rotella F, Lazarski K, Zhang R, Ginell S, Duke N, Naday I, Lazarz J, Molitsky M, Keefe L, Gonczy J, Rock L, Sanishvili R, Walsh M, Westbrook E, Joachimiak A (2006) The structural center 19ID undulator beamline: facility specifications and protein crystallographic results. J Sync Rad 13:30–45

Schmidt A, Lamzin V (2002) Veni, vidi, vici—atomic resolution unravelling the mysteries of protein function. Curr Opin Struct Biol 12:698–703

Shu F, Ramakrishnan V, Schoenborn B (2000) Enhanced visibility of hydrogen atoms by neutron crystallography on fully deuterated myoglobin. Proc Natl Acad Sci USA 97:3872–3877